The University of
Nottingham

UNITED KINGDOM · CHINA · MALAYSIA

Jäger, J.V. and Scherbakov, A.V. and Glavin, B.A. and Salasyuk, A.S. and Campion, R.P. and Rushforth, A.W. and Yakovlev, D.R. and Akimov, Andrey V. and Bayer, M. (2015) Resonant driving of magnetization precession in a ferromagnetic layer by coherent monochromatic phonons. Physcial Review B: Condensed matter and materials physics, 92 (2). 020404-1. ISSN 1550-235X

Access from the University of Nottingham repository:
http://eprints.nottingham.ac.uk/34350/1/Jager%20PhysRevB.92.020404.pdf

Copyright and reuse:

A note on versions:

Resonant driving of magnetization precession in a ferromagnetic layer by coherent monochromatic phonons

J. V. Jäger,[1] A. V. Scherbakov,[2] B. A. Glavin,[3] A. S. Salasyuk,[2] R. P. Campion,[4] A. W. Rushforth,[4] D. R. Yakovlev,[1,2] A. V. Akimov,[4] and M. Bayer[1,2]

[1]*Experimentelle Physik 2, Technische Universität Dortmund, D-44227 Dortmund, Germany*
[2]*Ioffe Physical-Technical Institute, Russian Academy of Science, 194021 St. Petersburg, Russia*
[3]*Department of Theoretical Physics, Lashkaryov Institute of Semiconductor Physics, 03028 Kiev, Ukraine*
[4]*School of Physics and Astronomy, University of Nottingham, Nottingham NG7 2RD, United Kingdom*
(Received 24 March 2015; published 16 July 2015)

We realize resonant driving of the magnetization precession by monochromatic phonons in a thin ferromagnetic layer embedded into a phononic Fabry-Pérot resonator. A femtosecond laser pulse excites resonant phonon modes of the structure in the $10-40$ GHz frequency range. By applying an external magnetic field, we tune the precession frequency relative to the frequency of the phonons localized in the cavity and observe an enormous increase in the amplitude of the magnetization precession when the frequencies of free magnetization precession and phonons localized in the cavity are equal.

The continual miniaturization of magnetic devices down to the nanometer scale has opened new horizons in data storage [1], computing [2,3], sensing [4,5], and medical technologies [6]. Progress in nanomagnetism is stimulated by emerging technologies, where methods to control magnetic excitations on the nanometer spatial and picosecond temporal scales include optical [7,8], electrical [8], and micromechanical [9] techniques. To realize ultrafast nanomagnetism on the technological level, new physical principles to efficiently induce and control magnetic excitations are required, and this remains a challenging task. A new basic approach to this problem would be to explore nanoscale magnetic resonance phenomena—resonant driving and monitoring of magnetic excitations—which is widely used nowadays in traditional magnetism for microscopy, medicine, and spectroscopy. The typical frequencies f_M of the magnetic resonances [e.g., the ferromagnetic resonance (FMR) in ferromagnetic and ferrimagnetic materials] are in the GHz and sub-THz frequency ranges. The traditional methods to scan magnetic excitations at these frequencies use microwaves, but due to the requirement of massive microwave resonators providing long wavelength radiation, they cannot provide high-speed control of magnetization locally on the nanoscale.

Among various emerging techniques in nanomagnetism, the application of stress to magnetostrictive ferromagnetic layers has been shown to be an effective, low-power method for controlling magnetization: Applying in-plane stress in stationary experiments enables irreversible switching of the magnetization vector [10]; the injection of picosecond strain pulses induces free precession of the magnetization [11]; excitation of quantized elastic waves in a membrane enables driving of the magnetization at GHz phonon frequencies [12]; and surface acoustic waves can be used to control the magnetic dynamics in ferromagnetic nanostructures [13–15]. In the present Rapid Communication, we examine the interaction of a high-frequency ($10-40$ GHz) magnetic resonance in a magnetostrictive ferromagnetic film with an elastic harmonic excitation in the form of a localized phonon mode, and demonstrate how this interaction becomes significantly stronger at resonance conditions.

Our device consists of a ferromagnetic layer embedded into a phonon Fabry-Pérot (FP) cavity. Such a cavity possesses quantized resonances for elastic waves (i.e., phonons) at frequencies f_{Ri} (i is the order of the phonon resonance). In the experiments, we excite these resonant modes optically by the methods of picosecond acoustics [16]. As it was shown earlier in experiments with picosecond strain pulses, coherent phonons induce free precession of the magnetization at the ferromagnetic resonance frequency f_M [11,17]. By the application of an external magnetic field **B**, we tune the frequency f_M into resonance with the phonon mode, $f_M = f_{Ri}$, and monitor the precession of the magnetization in the ferromagnetic layer. We observe an enormous increase of the magnetization precession lifetime and the spectral density at f_M when B corresponds to matching the resonant conditions of the magnetization precession and the phonon cavity mode.

The studied structure is shown schematically in Fig. 1(a). A 59-nm-thick ferromagnetic layer of Galfenol (alloy of 81% Fe and 19% Ga [18,19]) capped by a 3-nm Al layer (to prevent oxidation) is deposited by magnetron sputtering onto acoustic Bragg mirrors. These mirrors are formed by two superlattices (SL1 and SL2), each consisting of 10 periods of GaAs/AlAs bilayers with thicknesses (in nm) 59/71 and 42/49 in SL1 and SL2, respectively. The SLs are grown by molecular beam epitaxy on a semi-insulating (001) GaAs substrate. The Galfenol layer plays the role of a FP cavity between two flat phonon mirrors: One mirror is the free surface and the other is the corresponding SL1 or SL2 Bragg mirror. As SL2 is positioned below SL1, the cavity with the SL2 Bragg mirror therefore includes also all layers of SL1. The studied multilayer structure possesses a number of localized phonon modes with frequencies f_{Ri}, which fall into the stop bands of the SLs [20–22]. Figures 1(b) and 1(c) show the dispersion curves calculated for longitudinal (LA) phonons in the studied SL1 and SL2, respectively. The lowest phonon stop bands in SL1 and SL2 are centered at 20 and 28 GHz, respectively. The horizontal bars in the zoomed fragments of Figs. 1(b) and 1(c) indicate the calculated frequencies of the lowest phonon FP modes for the SL1 cavity ($f_{R1} = 20.0$ GHz) and the SL2 cavity
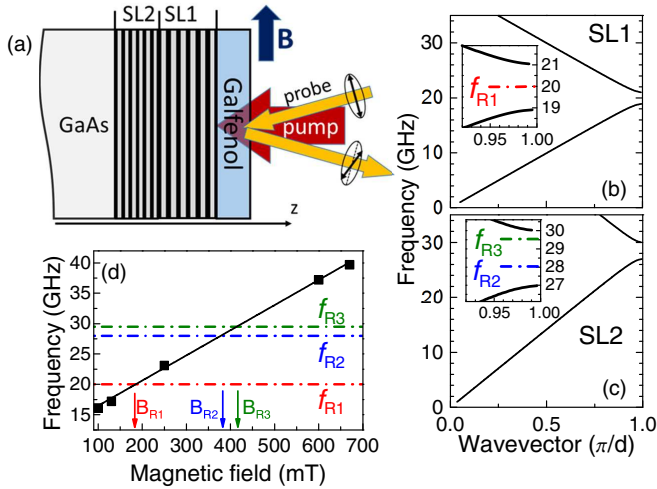
020404-1

FIG. 1. (Color online) (a) The scheme of excitation and detection of magnetization precession in a Galfenol layer grown on two phonon Bragg mirrors formed by GaAs/AlAs superlattices SL1 and SL2. (b), (c) Calculated phonon dispersion curves for two SL1 and SL2 Bragg mirrors, respectively. Horizontal bars in the zoomed insets indicate the frequency f_{Ri} of the phonon localized modes formed by the free surface and the corresponding SL Bragg mirror. (d) The magnetic field dependence of the free precession frequency f_M, measured (symbols) and linear fit (solid line). The horizontal lines show the spectral positions of the cavity phonon modes f_{Ri} and the vertical arrows indicate the corresponding resonance fields B_{Ri}.

($f_{R2} = 28.0$ GHz and $f_{R3} = 29.5$ GHz). The calculation of the FP phonon modes is described elsewhere [23].

Figure 1(d) shows these phonon modes as well as the magnetization precession frequency versus applied magnetic field for the studied sample. The squares show the measured dependence of the precession frequency in the studied Galfenol film on B, interpolated linearly by the solid line, which is in good agreement with previous experiments [19,24]. The horizontal dashed lines indicate the frequencies f_{Ri} of the phonon modes in the SL1 and SL2 cavities. The intersections of the solid and dashed lines give the resonances $f_M(B) = f_{Ri}$, which occur at particular resonance magnetic fields $B = B_{Ri}$, marked in Fig. 1(d) by the vertical arrows.

The experimental scheme is shown in Fig. 1(a). The FP phonon cavity with the Galfenol layer was excited by optical pump pulses from an amplified Ti:sapphire laser (duration 200 fs, wavelength of 800 nm, repetition rate 100 kHz) focused to a spot with a diameter 100 μm at the sample surface. The maximum energy density of the pump pulse was $\sim$10 mJ/cm^2. The probe pulses of lower density ($\sim$20 μJ/cm^2) split from the same laser and passed through an optical delay line were used to measure the transient magneto-optical Kerr rotation for monitoring the temporal evolution of the changes $\Delta M_z(t)$ of the z projection of the macroscopic magnetization **M** of the Galfenol layer, i.e., of the magnetization component normal to the surface [25]. The sample was mounted in a helium cryostat with a superconducting magnet. The experiments were performed at various temperatures up to room temperature, and most of the results presented here were obtained at $T = 170$ K. The external magnetic field up to 700 mT was applied in the
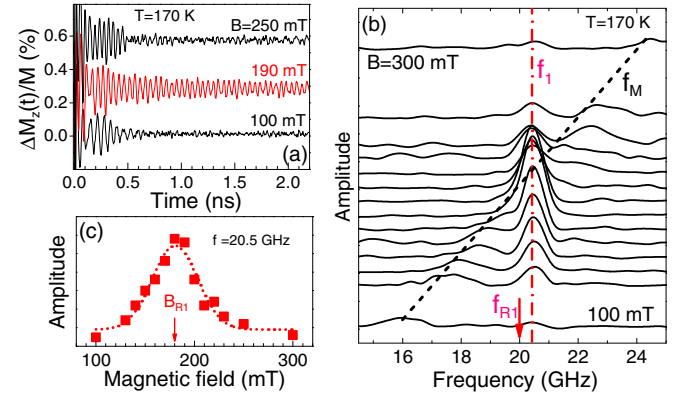

FIG. 2. (Color online) (a) Temporal evolution of the magnetization measured for three values of B. (b) The spectral density of the measured signals. The dashed vertical and oblique lines correspond to the maximum of the spectral line at $f_1 = 20.5$ GHz and the estimated position of the free magnetic precession f_M, respectively. The vertical arrow shows the calculated position of the lowest cavity mode f_{R1}. (c) Measured (symbols) dependence of the spectral amplitudes on the magnetic field for the spectral line centered at $f_1 = 20.5$ GHz, as indicated by the dashed vertical line in (b); the dotted line is the corresponding Gaussian fit of the experimental data. The vertical arrow shows the value of the resonant magnetic field $B_{R1} = 180$ mT.

plane of the Galfenol layer, **B**||[100], which is close to the easy magnetization axis [10,19].

The temporal evolution of the detected signals $\Delta M_z(t)$ measured for three values of B are shown in Fig. 2(a). The signals possess oscillatory behavior with the period, amplitude, and lifetime of the oscillations dependent on B. The most important result is the existence of a high-amplitude long-lived tail in the middle curve of Fig. 2(a) taken at $B = 190$ mT. This tail cannot be observed above the noise level at lower and higher fields (see the lower and upper curves, respectively).

To further inspect the data, we use a spectral domain presentation. Fast Fourier transform spectra (FFTs) of $\Delta M_z(t)$ for various B are shown in Fig. 2(b) in a frequency range 15−25 GHz. These spectra show a main spectral line centered at $f_1 = 20.5$ GHz, which, taking into account the accuracy of determining the SL parameters, may be unambiguously associated with the localized phonon mode in the FP cavity at $f_{R1} = 20.0$ GHz. The amplitude of this spectral line changes considerably with B: Figure 2(c) shows the B dependence of this amplitude where we clearly see that the amplitude maximum takes place at $B = 180$ mT. Figure 2(b) also shows a broader spectral line with lower amplitude whose position shifts to higher frequencies with an increase of B. This line corresponds to the fast decaying free precession of the magnetization with frequency close to f_M, whose B dependence for our Galfenol film is shown in Fig. 1(d). Comparing the coordinates of the first intersection in Fig. 1(d) with the data in Figs. 2(b) and 2(c), we conclude that the maximum amplitude in the spectra is obtained at $B \approx B_{R1}$. This observation is the main result of the present work and demonstrates a resonance in the magnetization precession that is driven by coherent phonons with frequency f_{R1}.

We now discuss the observed increase of the spectral density at $f_M = f_{Ri}$ in more detail. The optical pump pulse absorbed in the Galfenol layer results in an instantaneous rise of the layer temperature, generating a broad spectrum of coherent phonons in the form of a picosecond strain pulse [16]. The major fraction of generated phonons leaves the Galfenol film with a sound velocity on a time scale of $\sim$10 ps, but phonons with frequencies $f = f_{Ri}$ remain localized in the FP cavities for a longer time. The calculations for the cavity formed by SL1 at f_{R1} give a remarkably high value for the decay time of $\tau_{R1} \sim 10$ ns, which is three orders of magnitude longer than the escape time for nonresonant phonons from the cavity and two orders of magnitude longer than the lifetime of the free magnetization precession in this experimental geometry [19,24]. The localized phonons drive the magnetization precession at $f = f_{Ri}$, and this driving force will last during the leakage time τ_{R1}. The amplitude of the precession amplitude will increase when the resonance condition $f_M = f_{R1}$ is fulfilled. This is clearly observed in our experiments at $B = B_{R1} = 180$ mT for the signals measured in the temporal and spectral domains. The width Δf of the resonant curve in Fig. 2(c) is the same as the width of the spectral line for magnetization precession [19], which is in full agreement with the expectation for driving an object by a harmonic force. For nonresonant conditions, when B differs remarkably from B_{R1}, the low intensity spectral line at $f \approx f_M$ corresponds to the quickly decaying free oscillations due to the excitation of the magnetic precession by phonons from the initially generated broad spectrum and instantaneous temperature rise [17,26].

Thus, we conclude that the spectral amplitude of the magnetic precession at the frequency of the driving force rapidly increases at the resonance condition $f_M = f_{R1}$ for $B \approx B_{R1}$. To show the general validity of this statement, we perform further experiments for B values at which f_M falls into the region of the other two FP phonon modes of the SL2 cavity. In this case, the cavity, which comprises the Galfenol layer and SL1, has a length 1362 nm. The calculations for infinitely long SL2 predict two localized phonon states as shown in Fig. 1(c). Figure 3(a) shows the temporal evolution of $\Delta M_z(t)$ at $B = 400$ mT. The signal lasts longer than 6 ns (the time interval available for the experimental measurements) and possesses pronounced beatings due to simultaneous excitation of several spectral components. The corresponding spectral lines are clearly seen in the frequency domain presentation in Fig. 3(b). The frequencies of the peaks are independent of B, but their intensities vary strongly with B. The spectral lines with $f_2 = 28.4$ GHz and $f_3 = 30.0$ GHz show absolute maximal intensities in the magnetic field B interval between 350 and 450 mT. The frequencies of these two spectral lines are in good agreement with those of the calculated phonon modes $f_{R2} = 28.0$ GHz and $f_{R3} = 29.5$ GHz, and their maximum amplitudes are detected at the B values of the intersections in Fig. 1(d) demarking the resonance condition $f_M \approx f_{R2} \approx f_{R3}$. The origin of other lower amplitude spectral lines in Fig. 2(b) is the finite length of SL2. To confirm this, we have calculated the spectrum of the lattice displacement $G(\omega)$ near the surface assuming that light forming the excitation pulse is absorbed within a thickness $x_0 = 30$ nm of the Galfenol film. The resulting equation obtained in the spectral
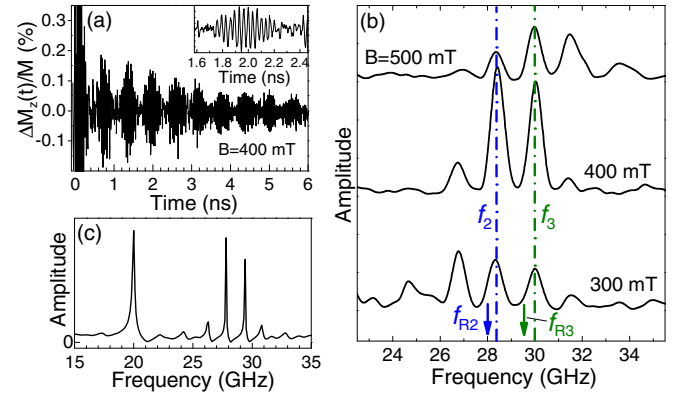

FIG. 3. (Color online) (a) Temporal evolution of the magnetization measured at $B = 400$ mT, when the long-lived tail with beatings has the maximum amplitude. The inset shows the zoomed fragment of the measured signal. (b) Spectral density of the measured signals for three values of the magnetic field. The vertical lines indicate the spectral positions f_2 and f_3 in the spectra of measured signals and the vertical arrows show the calculated frequencies f_{R2} and f_{R3}. (c) Calculated phonon spectrum for the studied structure for impulsive femtosecond optical excitation.

domain includes the multiple reflections of the generated strain pulse at all interfaces of the structure and may be written as

$$G(\omega) \sim \left| \frac{1}{1 + x_0^2 k_0^2} \left\{ i \frac{x_0 k_0 [1 + R(\omega)e^{2ik_0 d}]}{[1 - R(\omega)e^{2ik_0 d}]} + 1 \right\} \right|, \quad (1)$$

where $\omega = 2\pi f$, k_0 is the phonon wave vector in Galfenol, $d = 59$ nm is the thickness of the Galfenol film, and $R(\omega)$ is the complex reflectivity of the acoustic wave incident from the Galfenol on SL1 and SL2 grown on the GaAs substrate. $R(\omega)$ is calculated according to Ref. [23]. The result of the calculations based on Eq. (1) is shown in Fig. 3(c). Excellent agreement with the experiment is observed: There is a single line at $f = f_{R1} = 20$ GHz and a number of spectral lines in the region of 25−32 GHz exactly as observed experimentally. In fact, the appearance of the additional spectral lines is due to the phonon reflection resonances in finite-thickness SL existing at frequencies beyond but close to the edges of the phonon stop bands in a SL. Thus, we can conclude that resonant driving of the magnetization by coherent phonons also takes place for the SL2 cavity. The spectrum also consists of a visible nonzero background in the whole frequency range, which supplies the excitation of free precession at the nonresonant magnetic fields.

Finally, we discuss the possible role of transverse (TA) phonons in the studied nanostructure. In the experiments, we do not see any resonant effects at the B values that correspond to the resonance of f_M being equal to the frequency of localized TA phonons. This is not surprising because the optical pump excitation does not excite shear strain and correspondingly TA phonons in the present high symmetry geometry [27,28]. However, we could expect the generation of LA and TA phonons from the magnetization precession, as has been observed in conventional microwave-driven magnetoacoustic experiments [29]. Then the magnetic and elastic resonance would form a coupled magnetoelastic excitation, resulting in renormalization of the magnetic and phonon eigenstates [30].

The search for such excitations in ferromagnetic nanostructures is an extremely attractive field in nanomagnetism and nanomechanics.

In conclusion, we have demonstrated a method to drive resonantly the magnetization precession by sub-THz coherent phonons when the ferromagnetic layer is inserted into a phonon cavity. Resonant driving by coherent phonons can be used locally on the nanoscale and does not require external resonators, in contrast to microwave excitation. Nowadays it is possible to generate coherent monochromatic phonons optically up to frequencies of $\sim$1 THz [31–33], thus opening appealing perspectives for resonant driving of magnetic excitations possessing resonances at higher frequencies, e.g., in antiferromagnetic nanostructures. The interaction of high-frequency phonons and magnons on the nanoscale can lead to the development of a different class of devices.

For instance, the enhanced amplitude of the magnetization precession during resonant driving by coherent phonons shows the feasibility of precessional switching of the magnetization between metastable states [34].

[1] Y. Shiroishi, K. Fukuda, I. Tagawa, H. Iwasaki, S. Takenoiri, H. Tanaka, H. Mutoh, and N. Yoshikawa, Future options for HDD storage, IEEE Trans. Magn. **45**, 3816 (2009).

[2] A. Imre, G. Csaba, L. Ji, A. Orlov, G. H. Bernstein, and W. Porod, Majority logic gate for magnetic quantum-dot cellular automata, Science **311**, 205 (2006).

[3] D. Bhowmik, L. You, and S. Salahuddin, Spin Hall effect clocking of nanomagnetic logic without a magnetic field, Nat. Nanotechnol. **9**, 59 (2014).

[4] J. R. Maze, P. L. Stanwix, J. S. Hodges, S. Hong, J. M. Taylor, P. Cappellaro, L. Jiang, M. V. Gurudev-Dutt, E. Toga1, A. S. Zibrov, A. Yacoby, R. L. Walsworth, and M. D. Lukin, Nanoscale magnetic sensing with an individual electronic spin in diamond, Nature (London) **455**, 644 (2008).

[5] I. K. Kominis, T. W. Kornack, J. C. Allred, and M. V. Romalis, A subfemtotesla multichannel atomic magnetometer, Nature (London) **422**, 596 (2003).

[6] E. A. Vitol, V. Novosad, and E. A. Rozhkova, Microfabricated magnetic structures for future medicine: From sensors to cell actuators, Nanomedicine **7**, 1611 (2015).

[7] A. Kirilyuk, A. V. Kimel, and T. Rasing, Ultrafast optical manipulation of magnetic order, Rev. Mod. Phys. **82**, 2731 (2010), and references therein.

[8] N. Locatelli, V. Cros, and J. Grollier, Spin-torque building blocks, Nat. Mater. **13**, 11 (2014).

[9] E. R. MacQuarrie, T. A. Gosavi, N. R. Jungwirth, S. A. Bhave, and G. D. Fuchs, Mechanical spin control of nitrogen-vacancy centers in diamond, Phys. Rev. Lett. **111**, 227602 (2013).

[10] D. E. Parkes, S. A. Cavill, A. T. Hindmarch, P. Wadley, F. McGee, C. R. Staddon, K. W. Edmonds, R. P. Campion, B. L. Gallagher, and A. W. Rushforth, Non-volatile voltage control of magnetization and magnetic domain walls in magnetostrictive epitaxial thin films, Appl. Phys. Lett. **101**, 072402 (2012).

[11] A. V. Scherbakov, A. S. Salasyuk, A. V. Akimov, X. Liu, M. Bombeck, C. Bruggemann, D. R. Yakovlev, V. F.Sapega, J. K. Furdyna, and M. Bayer, Coherent magnetization precession in ferromagnetic (Ga,Mn)As induced by picosecond acoustic pulses, Phys. Rev. Lett. **105**, 117204 (2010).

[12] D. Afanasiev, I. Razdolski, K. M. Skibinsky, D. Bolotin, S. V. Yagupov, M. B. Strugatsky, A. Kirilyuk, Th. Rasing, and A. V. Kimel, Laser excitation of lattice-driven anharmonic magnetization dynamics in dielectric $FeBO_3$, Phys. Rev. Lett. **112**, 147403 (2014).

[13] S. Davis, A. Baruth, and S. Adenwalla, Magnetization dynamics triggered by surface acoustic waves, Appl. Phys. Lett. **97**, 232507 (2010).

[14] Y. Yahagi, B. Harteneck, S. Cabrini, and H. Schmidt, Controlling nanomagnet magnetization dynamics via magnetoelastic coupling, Phys. Rev. B **90**, 140405(R) (2014).

[15] J. Janušonis, C. L. Chang, P. H. M. van Loosdrecht, and R. I. Tobey, Frequency tunable surface magneto elastic waves, Appl. Phys. Lett. **106**, 181601 (2015).

[16] C. Thomsen, H. T. Grahn, H. J. Maris, and J. Tauc, Surface generation and detection of phonons by picosecond light pulses, Phys. Rev. B **34**, 4129 (1986).

[17] J.-W. Kim, M. Vomir, and J.-Y. Bigot, Ultrafast magnetoacoustics in nickel films, Phys. Rev. Lett. **109**, 166601 (2012).

[18] A. E. Clark, K. B. Hathaway, M. Wun-Fogle, J. B. Restorff, Thomas A. Lograsso, V. M. Keppens, G. Petculescu, and R. A. Taylor, Extraordinary magnetoelasticity and lattice softening in bcc Fe-Ga alloys, J. Appl. Phys. **93**, 8621 (2003).

[19] D. E. Parkes, L. R. Shelford, P. Wadley, V. Holý, M. Wang, A. T. Hindmarch, G. van der Laan, R. P. Campion, K. W. Edmonds, S. A. Cavill, and A. W. Rushforth, Magnetostrictive thin films for microwave spintronics, Sci. Rep. **3**, 2220 (2013).

[20] W. Chen, Y. Lu, H. J. Maris, and G. Xiao, Picosecond ultrasonic study of localized phonon surface modes in Al/Ag superlattices, Phys. Rev. B **50**, 14506 (1994).

[21] M. Trigo, T. A. Eckhause, M. Reason, R. S. Goldman, and R. Merlin, Observation of surface-avoiding waves: A new class of extended states in periodic media, Phys. Rev. Lett. **97**, 124301 (2006).

[22] M. F. Pascual Winter, G. Rozas, A. Fainstein, B. Jusserand, B. Perrin, A. Huynh, P. O. Vaccaro, and S. Saravanan, Selective optical generation of coherent acoustic nanocavity modes, Phys. Rev. Lett. **98**, 265501 (2007).

[23] S. Mizuno and S.-I. Tamura, Theory of acoustic-phonon transmission in finite-size superlattice systems, Phys. Rev. B **45**, 734 (1992).

[24] J. V. Jäger, A. V. Scherbakov, T. L. Linnik, D. R. Yakovlev, M. Wang, P. Wadley, V. Holy, S. A. Cavill, A. V. Akimov, A. W. Rushforth, and M. Bayer, Picosecond inverse magnetostriction in galfenol thin films, Appl. Phys. Lett. **103**, 032409 (2013).

[25] W. K. Hiebert, A. Stankiewicz, and M. R. Freeman, Direct observation of magnetic relaxation in a small permalloy disk by time-resolved scanning kerr microscopy, Phys. Rev. Lett. **79**, 1134 (1997).

[26] H. B. Zhao, D. Talbayev, Q. G. Yang, G. Lüpkea, A. T. Hanbicki, C. H. Li, O. M. J. van't Erve, G. Kioseoglou, and B. T. Jonker, Ultrafast magnetization dynamics of epitaxial Fe films on AlGaAs (001), Appl. Phys. Lett. **86**, 152512 (2005).

[27] T. Pezeril, P. Ruello, S. Gougeon, N. Chigarev, D. Mounier, J.-M. Breteau, P. Picart, and V. Gusev, Generation and detection of plane coherent shear picosecond acoustic pulses by lasers: Experiment and theory, Phys. Rev. B **75**, 174307 (2007).

[28] O. Matsuda, O. B. Wright, D. H. Hurley, V. Gusev, and K. Shimizu, Coherent shear phonon generation and detection with picosecond laser acoustics, Phys. Rev. B **77**, 224110 (2008).

[29] J. W. Tucker and V. W. Rampton, *Microwave Ultrasonics in Solid State Physics* (North-Holland, Amsterdam, 1972).

[30] H. Matthews and R. C. LeCraw, Acoustic wave rotation by magnon-phonon interaction, Phys. Rev. Lett. **8**, 397 (1962).

[31] A. Bartels, T. Dekorsy, H. Kurz, and K. Köhler, Coherent zone-folded longitudinal acoustic phonons in semiconductor superlattices: Excitation and detection, Phys. Rev. Lett. **82**, 1044 (1999).

[32] C.-K. Sun, J.-C. Liang, and X.-Y. Yu, Coherent acoustic phonon oscillations in semiconductor multiple quantum wells with piezoelectric fields, Phys. Rev. Lett **84**, 179 (2000).

[33] A. Huynh, B. Perrin, and A. Lemaître, Coherent acoustic phonon oscillations in semiconductor multiple quantum wells with piezoelectric fields, Ultrasonics **56**, 66 (2015).

[34] L. Thevenard, J.-Y. Duquesne, E. Peronne, H. J. von Bardeleben, H. Jaffres, S. Ruttala, J.-M. George, A. Lemaître, and C. Gourdon, Irreversible magnetization switching using surface acoustic waves, Phys. Rev. B **87**, 144402 (2013).